

Nuclear effects in neutrino-nucleus DIS

M. Hirai*, S. Kumano[†] and K. Saito*

**Department of Physics, Faculty of Science and Technology, Tokyo University of Science
2641, Yamazaki, Noda, Chiba, 278-8510, Japan*

*[†]KEK Theory Center, Institute of Particle and Nuclear Studies, KEK
and Department of Particle and Nuclear Studies, Graduate University for Advanced Studies
1-1, Oho, Tsukuba, Ibaraki, 305-0801, Japan*

Abstract. We explain the current status of nuclear parton distribution functions in connection with neutrino-nucleus interactions. Neutrino deep inelastic scattering (DIS) measurements have been done for heavy nuclear targets such as iron and lead. In order to extract structure functions of the nucleon, one needs to remove nuclear effects from the data. However, recent studies indicate that there are inconsistencies in nuclear modifications between charged-lepton and neutrino scattering measurements. Nuclear medium effects could be also an origin for the NuTeV anomaly in the weak-mixing angle. In addition, the modifications could affect neutrino-oscillation experiments because some DIS events of neutrino-oxygen nucleus interactions are contained. On the other hand, the nuclear medium effects themselves are interesting and important for describing nuclei in terms of quark and gluon degrees of freedom.

Keywords: Neutrino, quark, gluon, parton distribution, QCD, nuclear effect

PACS: 13.15.+g, 13.60.Hb, 24.85.+p, 12.38.-t

INTRODUCTION

Nuclear modifications of structure functions were found in charged-lepton deep inelastic scattering (DIS) by the European Muon Collaboration (EMC) [1], so that they are often called the EMC effect. Since nuclear binding energies per nucleon are much smaller than a typical DIS scale, such effects were not expected except for possible Fermi-motion effects. Later, the nuclear effects are interpreted mainly by binding and Fermi-motion mechanisms with possible internal modifications of the nucleon at medium and large x [2]. At small x , suppression is observed in the structure functions, and the phenomenon is called shadowing which is understood by multiple scattering of $q\bar{q}$ -like states originating from a virtual photon. The reader may look at a summary article in Ref. [3] for explanations of these mechanisms.

On the other hand, there are growing interests in nuclear effects in neutrino DIS structure functions with the following reasons.

1. Current neutrino DIS measurements contain nuclear medium effects because heavy nuclear targets, iron and lead, are used. Neutrino data are valuable especially for determining valence-quark distributions in the nucleon because the parity-violating F_3 structure function directly probes the valence distributions. However, the nuclear effects should be properly removed from the neutrino measurements for extracting information on the nucleonic parton distribution functions (PDFs) [4].
2. There is an issue of NuTeV anomaly on the weak-mixing angle $\sin^2 \theta_W$ [5]. It could be related to a nuclear medium effect in the iron nucleus [6].

3. For neutrino oscillation measurements, nuclear effects need to be understood for neutrino-oxygen nucleus reactions [7]. Although such experiments are not at very high energies, they contain a certain number of DIS events. In order to understand the DIS as well as a resonance region, quark-hadron duality should be studied for extending the knowledge of nuclear DIS to a relatively low-energy region [8].

In order to determine nuclear effects in general, a global χ^2 analysis method was developed in Ref. [9] by using all the available charged-lepton DIS data, and then by adding Drell-Yan data to the data set [10]. Subsequently, there have been various proposals for the optimum nuclear PDFs. Here, we explain recent progress on the various global analyses [11, 12, 13, 14, 15, 16]. Nuclear parton distributions have been determined in Refs. [11, 12, 13, 14], whereas Ref. [15] focused on structure functions by using conventional nuclear models and Ref. [16] especially on the shadowing part.

STRUCTURE FUNCTIONS IN NEUTRINO DIS

Neutrino charged-current interactions with the nucleon are described by the matrix element

$$M = \frac{G_F/\sqrt{2}}{1 + Q^2/M_W^2} \bar{u}(k', \lambda') \gamma^\mu (1 - \gamma_5) u(k, \lambda) \langle X | J_\mu^{CC}(0) | p, \lambda_N \rangle, \quad (1)$$

where G_F is the Fermi coupling constant, M_W is the W mass, Q^2 is given by $Q^2 = -q^2$ with the four-momentum transfer q , k (λ) and k' (λ') indicate initial and final lepton momenta (spins), p (λ_N) is the nucleon momentum (spin), and $J_\mu^{CC}(0)$ is the weak charged current (CC) of the nucleon. The absolute-value square $|M|^2$ is calculated with an average over the nucleon spin for obtaining the unpolarized cross section. The leptonic part is calculated and the hadronic part becomes the hadron tensor $W_{\mu\nu}^{CC}$, which is then expressed by three structure functions F_1 , F_2 , and F_3 :

$$\left(\frac{d\sigma}{dx dy} \right)_{CC}^{v, \bar{v}} = \frac{G_F^2 M_N E}{\pi (1 + Q^2/M_W^2)^2} \left[F_1^{cc} x y^2 + F_2^{cc} \left(1 - y - \frac{M_N x y}{2E} \right) \pm F_3^{cc} x y \left(1 - \frac{y}{2} \right) \right], \quad (2)$$

where \pm indicates $+$ for v and $-$ for \bar{v} , s is the center-of-mass energy squared, x is the Bjorken scaling variable $x = Q^2/(2p \cdot q)$, y is defined by $y = p \cdot q/(p \cdot k)$, E is the neutrino-beam energy, and M_N is the nucleon mass. The cross section is calculated in a quark-parton model to express the structure functions in terms of parton distribution functions (PDFs):

$$\begin{aligned} F_2 &= 2xF_1, & F_2^{vP} &= 2x(d + s + \bar{u} + \bar{c}), & F_2^{\bar{v}P} &= 2x(u + c + \bar{d} + \bar{s}), \\ xF_3^{vP} &= 2x(d + s - \bar{u} - \bar{c}), & xF_3^{\bar{v}P} &= 2x(u + c - \bar{d} - \bar{s}), \end{aligned} \quad (3)$$

in the leading twist and the leading order of the running coupling constant α_s . These equations are combined to become

$$F_3^{vP} + F_3^{\bar{v}P} = 2(u_v + d_v) + 2(s - \bar{s}) + 2(c - \bar{c}), \quad (4)$$

for the structure functions F_3 . It indicates that measurements of F_3 are valuable for determining the valence-quark distributions in the nucleon because $s - \bar{s}$ and $c - \bar{c}$ are

considered to be very small. Another important point of neutrino DIS is to determine the strange quark ratio to the light-quark ones $2\bar{s}/(\bar{u} + \bar{d})$ by using neutrino-induced opposite-sign dimuon events ($\nu_{\mu}P \rightarrow \mu^+\mu^-X$) by assuming a charm-quark production process.

Recent neutrino DIS experiments are listed in Table 1 [17, 18, 19]. These measurements have been done for heavy nuclear targets of iron and lead. In order to extract the structure functions of the nucleon, one needs to remove nuclear medium effects, which may be assumed to be the same as the ones for the charged-lepton scattering. However, nuclear modifications are generally different from the ones in the charged-lepton DIS. We discuss these nuclear medium effects in this article. In the near future, the MINERvA collaboration will measure the nuclear structure functions for the targets, helium, carbon, iron, and lead [20]. Their measurements should provide valuable information for clarifying the nuclear effects in neutrino reactions.

TABLE 1. Recent neutrino DIS experiments

Experiment	Target	ν energy (GeV)
CCFR	Fe	30–360
CDHSW	Fe	20–212
CHORUS	Pb	10–200
NuTeV	Fe	30–500

In Fig. 1, data are shown for the Q^2 dependence of the structure functions F_2 and F_3 [19] of NuTeV, CCFR, and CDHSW measurements together with NuTeV fit curves. We notice that the minimum x is about 0.01 for $Q^2 > 1 \text{ GeV}^2$ due to fixed target measurements in comparison with HERA collider data of $x_{min} \sim 10^{-4}$. Therefore, the current neutrino data are valuable for determining the PDFs at medium and large x ($0.01 < x < 0.8$). As shown in Eq. (3), neutrino reactions provide information on quark flavor separations which are different from the charged-lepton ones.

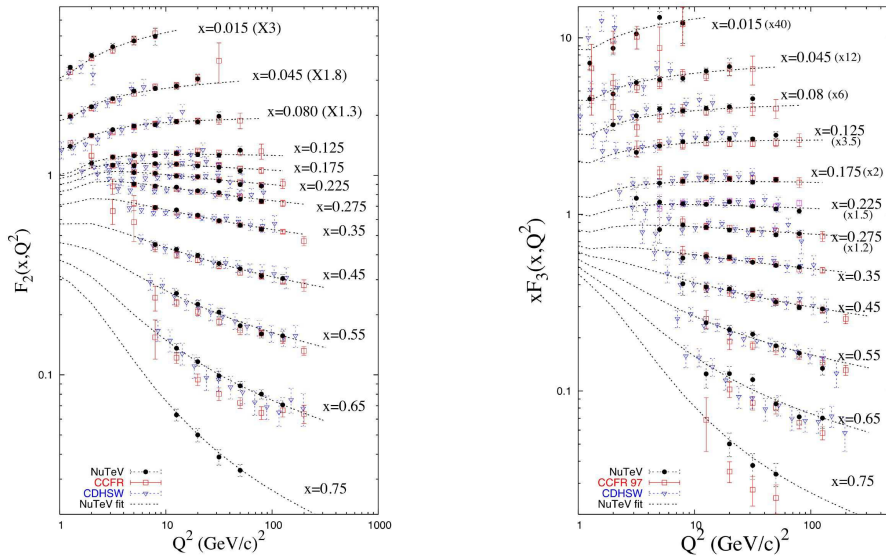


FIGURE 1. Structure functions F_2 and F_3 in neutrino deep inelastic scattering [19].

DETERMINATION OF NUCLEAR PDFS

Nucleonic PDFs and nuclear modifications

The structure functions F_2 and F_3 are expressed in terms of the PDFs, which are then convoluted with coefficient functions for taking into account higher-order effects of α_s . The PDFs of the nucleon have been investigated for a long time. Because of a variety of experimental measurements such as charged-lepton DIS, neutrino DIS, Drell-Yan, W and jet production processes, etc. and also established theoretical analysis techniques, the PDFs are now precisely determined from small to relatively large x . A typical situation is shown in Fig. 2 at $Q^2=10 \text{ GeV}^2$. Uncertainties of the PDFs are shown by the bands in the figure. They indicate that the distributions are well determined in the wide range of x . Relative uncertainties ($\delta f/f$) are large at large x (> 0.5) although they are not conspicuous in Fig. 2 because the distributions themselves are small.

Typical measurements on nuclear modifications of F_2 in charged-lepton scattering are shown for the carbon nucleus as an example in Fig. 3, where the ratio F_2^C/F_2^D is shown [12, 21]. Here, C and D indicate the carbon nucleus and the deuteron. The JLab data at large x (> 0.8) have small invariant masses ($W^2 < 3 \text{ GeV}^2$) [21], so that they are not considered to be obtained in the DIS process. Physics mechanisms for these nuclear medium effects are explained in Ref. [3]. At large x (> 0.7), the ratio tends to increase with x , which is caused by nucleon's Fermi motion in a nucleus. At medium x ($0.2 < x < 0.6$), main effects come from nuclear binding possibly together with internal nucleon modifications in a nuclear medium [2]. The Fermi-motion and binding effects are theoretically calculated in a convolution model. The nuclear structure function F_2^A is given by the free nucleonic one F_2^N convoluted with a nucleon energy-momentum distribution, which is called a spectral function, in a nuclear medium. At small x ($x < 0.1$), the suppression of the ratio is caused by shadowing, which is described by multiple scattering of $q\bar{q}$ -like configuration of the virtual photon. The enhancement at $x \sim 0.15$ is called antishadowing. It should be caused by the conservations of baryon number and charge of a nucleus, but there is an attempt to attribute it to a constructive interference effect in Pomeron and Reggeon exchanges [22].

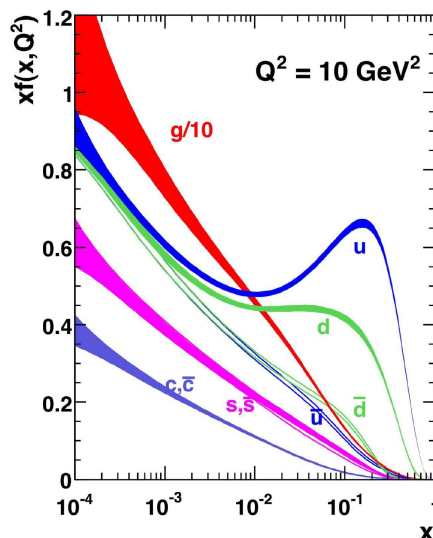


FIGURE 2: PDFs in the nucleon [4]

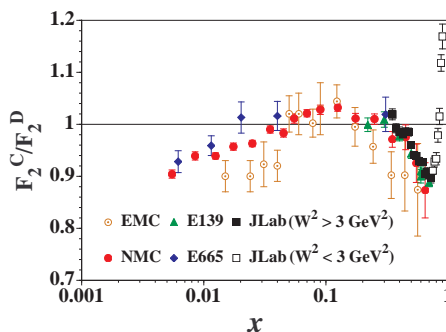


FIGURE 3: Nuclear modifications of F_2

Analysis method for nuclear PDFs

We explain global-analysis methods for determining nuclear PDFs. A nucleus consists of mainly protons and neutrons although the existence of mesons needs to be considered. Therefore, it is appropriate to assume that a NPDF (nuclear PDFs) $f_i^A(x)$ for the parton type i is given by proton and neutron contributions as the first approximation, and then their nuclear modifications are addressed, for example, in the following functional form [9, 10]:

$$f_i^A(x, Q_0^2) = w_i(x, A, Z) \frac{1}{A} [Z f_i^p(x, Q_0^2) + (A - Z) f_i^n(x, Q_0^2)], \quad (5)$$

where p and n indicate the proton and neutron, and Q_0^2 is the initial Q^2 scale. The isospin symmetry ($u \equiv d^n = u^p$, $d \equiv u^n = d^p$) is assumed in relating the distributions in the neutron to the ones in the proton. The x -dependent functional form is not unique. In the following, some recent parametrizations are shown as examples:

- DS04[11] ($Q_0^2 = 0.4 \text{ GeV}^2$): $f_i^{N/A}(x) = \int \frac{dy}{y} W_i(y, A, Z) f_i^N(x/y)$,

$$W_i(y, A, Z) = \begin{cases} A [a_v \delta(1 - \varepsilon_v - y) + (1 - a_v) \delta(1 - \varepsilon_v - y)] \\ \quad + n_v \left(\frac{y}{A}\right)^{\alpha_v} \left(1 - \frac{y}{A}\right)^{\beta_v} + n_s \left(\frac{y}{A}\right)^{\alpha_s} \left(1 - \frac{y}{A}\right)^{\beta_s} & (i = V), \\ A \delta(1 - y) + \frac{a_i}{N_i} \left(\frac{y}{A}\right)^{\alpha_i} \left(1 - \frac{y}{A}\right)^{\beta_i} & (i = s, g) \end{cases} \quad (6)$$

- HKN07[12] ($Q_0^2 = 1 \text{ GeV}^2$): $f_i^A(x) = w_i(x, A, Z) \frac{1}{A} [Z f_a^p(x) + (A - Z) f_a^n(x)]$,

$$w_i(x, A, Z) = 1 + \left(1 - \frac{1}{A^\alpha}\right) \frac{a_i + b_i x + c_i x^2 + d_i x^3}{(1 - x)^\beta}, \quad (7)$$

- SYKMOO08[13] ($Q_0^2 = 1.69 \text{ GeV}^2$): $f_i^A(x) = \frac{1}{A} [Z f_a^{p/A}(x) + (A - Z) f_a^{n/A}(x)]$,

$$x f_i^{N/A}(x) = \begin{cases} A_0 x^{A_1} (1 - x)^{A_2} e^{A_3 x} (1 + e^{A_4 x})^{A_5} & (i = u_v, d_v, g, \bar{u} + \bar{d}, \bar{s}) \\ A_0 x^{A_1} (1 - x)^{A_2} + (1 + A_3 x) (1 - x)^{A_4} & (i = \bar{d}/\bar{u}), \end{cases} \quad (8)$$

- EPS09[14] ($Q_0^2 = 1.69 \text{ GeV}^2$): $f_i^A(x) = R_i^A(x) \frac{1}{A} [Z f_a^p(x) + (A - Z) f_a^n(x)]$,

$$R_i^A(x) = \begin{cases} a_0 + (a_1 + a_2 x)[e^{-x} - e^{-x a}] & (x \leq x_a : \text{shadowing}) \\ b_0 + b_1 x + b_2 x^2 + b_3 x^3 & (x_a \leq x \leq x_e : \text{antishadowing}). \\ c_0 + (c_1 - c_2 x)(1 - x)^{-\beta} & (x_e \leq x \leq 1 : \text{EMC \& Fermi}) \end{cases} \quad (9)$$

The parameters in these equations are determined by global χ^2 analyses of world experimental data on nuclear structure functions. Experimental data are generally obtained in different Q^2 points from Q_0^2 . The standard DGLAP evolution equations are used for evolving the distributions to the experimental points. There are three conditions to be satisfied for the NPDFs, so that three parameters should be fixed by the following relations [9, 10]:

$$\begin{aligned} \text{Baryon number: } & A \int dx \left[\frac{1}{3} u_v^A(x) + \frac{1}{3} d_v^A(x) \right] = A, \\ \text{Charge: } & A \int dx \left[\frac{2}{3} u_v^A(x) - \frac{1}{3} d_v^A(x) \right] = Z, \\ \text{Momentum: } & A \sum_{i=q, \bar{q}, g} \int dx x f_i^A(x) = A. \end{aligned} \quad (10)$$

In the global analysis for the NPDFs, available data are still limited. Furthermore, final-state interactions could affect cross sections of hadron productions in nuclear reactions, and there are uncertainties coming from fragmentation functions and their nuclear modifications. The data used for the analyses are shown in Table 2. There are measurements of the structure function ratios $F_2^A/F_2^{A'}$, Drell-Yan cross section ratios $\sigma_{DY}^{pA}/\sigma_{DY}^{pA'}$, and pion-production ratios $\sigma_\pi^{dA}/\sigma_\pi^{pp}$ of RHIC. The data sets used in the analyses, DS04, HKN07, and EPS09 are shown in Table 2. The DS04 and EPS09 are somewhat selective on the data sets. The numbers in the parentheses of EPS09 indicate weight factors in calculating the total χ^2 . For example, the pion-production measurements of RHIC are amplified with the weight factor 20.

The kinematical (x, Q^2) range of F_2 and Drell-Yan data is shown in Fig. 4. These data are taken by fixed-target experiments, so that the range is limited, for example, in comparison with the collider data of HERA. In future, the kinematical range will be extended by Drell-Yan measurements at RHIC and LHC, and also by the possible EIC (electron-ion collider) project.

A difference from the kinematical range ($0 < x < 1$) of the nucleonic PDFs is that there exists a region $x > 1$ for the NPDFs. If the scaling variable is defined by $x_A = Q^2/(2M_A v)$ with the target nuclear mass M_A and the energy transfer v , it is certainly restricted by $0 < x_A < 1$. However, experimental measurements are usually published by the Bjorken scaling variable $x = Q^2/(2M_N v)$ even for nuclei, so that the range of x becomes $0 < x < A$ because of the mass ratio $M_A/M_N \approx A$. However, the extremely large- x region ($x > 1$) is neglected in current global analyses because there is no DIS data with $W^2 > 3 \text{ GeV}^2$ as shown in Fig. 3 and the structure functions are very small in this region.

From the χ^2 fit to these data, the optimum values and their errors are determined for the parameters of the NPDFs at Q_0^2 . Uncertainties of the NPDFs are estimated from the global analyses. Popular methods are the Hessian and the Lagrange-multiplier methods.

We comment on the Kulagin and Petti's analysis [15]. Their approach is quite different from the above ones in the sense that they try to calculate the nuclear corrections in conventional nuclear models as far as they can, and then they try to attribute remaining factors to off-shell effects of bound nucleons for explaining the data. This off-shell part is parametrized and is determined by analysis of nuclear structure functions.

R	Nucleus	Experiment	EPS09	HKN07	DS04		
DIS	A/D	D/p	NMC	0	0	0	
		4He	SLAC E139	0	0	0	
			NMC95	0 (5)	0	0	
		Li	NMC95	0	0	0	
		Be	SLAC E139	0	0	0	
		C	EMC-88_90		0	0	0
			NMC 95		0	0	0
			SLAC E139		0	0	0
			FNAL-E865		0	0	0
		N	BCDMS 85		0	0	0
	HERMES 03			0	0	0	
	Al	SLAC E49		0	0	0	
		SLAC E139		0	0	0	
	Ca	EMC 90		0	0	0	
		NMC 95		0	0	0	
		SLAC E139		0	0	0	
		FNAL-E865		0	0	0	
	Fe	SLAC E87		0	0	0	
		SLAC E139		0 (15)	0	0	
		SLAC E140		0	0	0	
		BCDMS 87		0	0	0	
	Cu	EMC 93		0	0	0	
		HERMES 03		0	0	0	
		SLAC E139		0	0	0	
		EMC 88		0	0	0	
	Au	SLAC E139		0	0	0	
		SLAC E140		0	0	0	
	Pb	FNAL-E865		0	0	0	
		NMC 96		0	0	0	
	A/C	Al	NMC 95	0	0	0	
Ca		NMC 95	0	0	0		
Fe		NMC 96	0	0	0		
Sn		NMC 96	0 (10)	0	0		
Pb		NMC 96	0	0	0		
C		NMC 95	0	0	0		
A/Li	Ca	NMC 95	0	0	0		
	C		0	0	0		
	Ca	FNAL-E772	0 (15)	0	0		
	Fe		0 (15)	0	0		
DY	W		0 (10)	0	0		
	Fe		0	0	0		
A/Be	W	FNAL E866	0	0	0		
	W		0	0	0		
pp	dA/pp	Au	RHIC-PHENIX	0 (20)	0		

TABLE 2: Data for global analysis

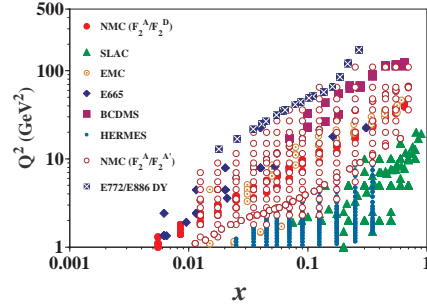


FIGURE 4: Kinematical range of data [10]

Nuclear PDFs and their uncertainties

Nuclear PDFs are determined by the data mainly on the F_2 ratios and the Drell-Yan cross section ratios. Total $\chi^2/\text{d.o.f.}$ are 0.76 (DS04), 1.2 (HKN07), 1.4 (SYKMOO08), and 0.80 (EPS09). In the SYKMOO08 analysis, only the neutrino data are used. Typical results are shown in Fig. 5 for the calcium nucleus. Here, the nuclear modifications w_i in Eq. (5) are shown for valence-quark, antiquark, and gluon distributions at $Q^2=1 \text{ GeV}^2$ [12]. Both leading order (LO) and next-to-leading order (NLO) results are shown by the solid and dashed curves, respectively. Their uncertainty ranges are shown by the shaded bands.

The figure indicates that the uncertainties are slightly smaller in the NLO especially in antiquark and gluon distributions. The results show that the valence-quark distributions are well determined due to the accurate measurements of the F_2 modifications at medium x in the charged-lepton DIS. The antishadowing of F_2 should be interpreted by the enhancement of the valence-quark distributions at $x \sim 0.15$ because modifications are small for antiquark distributions according to Fermilab Drell-Yan measurements. The small- x behavior of $w^A(x)$ for the valence quarks is constrained by the baryon-number and charge conservations. The antiquark modifications are also well determined at small x (< 0.1); however, there are large uncertainties at $x > 0.2$. This issue will be clarified in the near future by the Fermilab E906 [23] and a possible J-PARC Drell-Yan experiments [24]. The antiquark modifications are still assumed to be flavor symmetric [25]. The gluon modifications are not determined well in the whole- x range. We need accurate measurements on direct-photon and jet productions at RHIC and LHC.

We show the results for the lead nucleus and comparison of various NPDF results in Fig. 6 [14]. Nuclear modifications are shown for the valence-quark, sea-quark, and gluon distributions (R_V^{Pb} , R_S^{Pb} , R_G^{Pb}) at $Q^2=1.69 \text{ GeV}^2$ and 100 GeV^2 . All the analyses results (DS04, HKN07, EPS09) are shown in the NLO. The uncertainty regions of the EPS09 are indicated by the shaded bands. All the three analyses use similar data sets as shown in Table 2. The functional forms are slightly different in these models. However, irrespective of these differences, the three modifications are roughly within the error bands, which indicates consistency of these results.

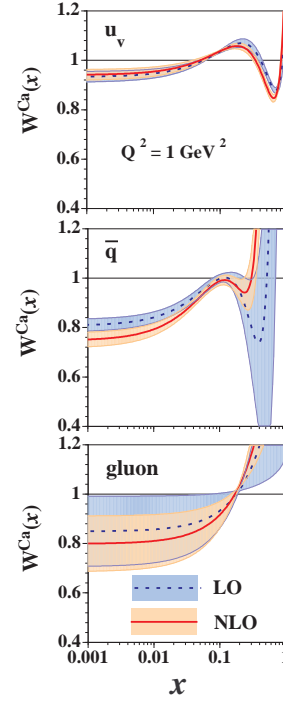


FIGURE 5: Modifications in calcium

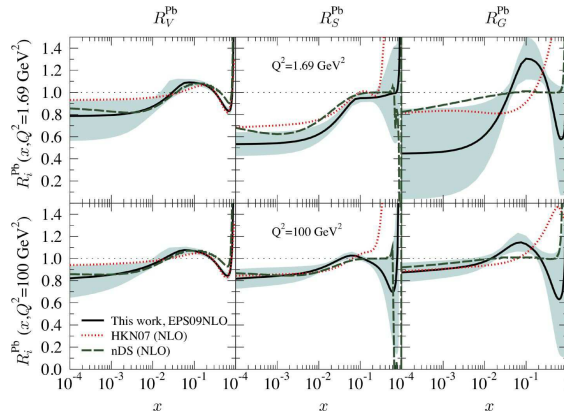


FIGURE 6: Modifications in lead [14]

In the analyses of Figs. 5 and 6, neutrino data are not included. In Ref. [13], a global analysis was done for the neutrino data. A typical result is shown as the “fit A2” in Fig. 7 for the modifications of F_2^{vFe} in comparison with a charged-lepton modification curve (SLAC/NMC) and other analysis results (KP and HKN07). Obviously, there are unexpected differences between the modifications of charged lepton and neutrino reactions. The medium- x depletion is smaller in the neutrino scattering, and the antishadowing region is shifted toward a smaller- x region. Because the neutrino DIS data are corrected mostly by assuming both nuclear modifications are the same, this discrepancy poses a question on the precision of current nucleonic PDFs by using neutrino DIS data for the nuclear targets. A similar discrepancy was reported by the recent MSTW analysis [4], so that it should be clarified by future theoretical and experimental investigations.

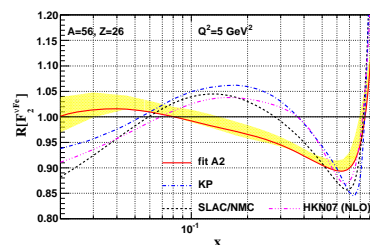


FIGURE 7: Modifications in charged-lepton and neutrino scattering off iron [13]

ACKNOWLEDGMENTS

The authors would like to thank M. Sakuda for his support on this project. They thank D. Naples, C. A. Salgado, I. Schienbein, G. Watt, American Physical Society, European Physics Journal, and Journal of High Energy Physics for permitting them to use figures.

REFERENCES

1. J. Ashman *et al.* (European Muon Collaboration (EMC)), *Phys. Lett. B* **202**, 603 (1988).
2. K. Saito and A.W. Thomas, *Nucl. Phys. A* **574**, 659 (1994); I. C. Cloet, W. Bentz, and A. W. Thomas, *Phys. Lett. B* **642**, 210 (2006).
3. D. F. Geesaman, K. Saito, and A. W. Thomas, *Ann. Rev. Nucl. Part. Sci.* **45**, 337 (1995).
4. A. D. Martin, W. J. Stirling, R. S. Thorne, and G. Watt, arXiv: 0901.0002 (*Eur. Phys. J.* in press).
5. G. P. Zeller *et al.* (NuTeV Collaboration), *Phys. Rev. Lett.* **88**, 091802 (2002); **90**, 239902 (2003).
6. S. Kumano, *Phys. Rev. D* **66**, 111301 (2002); M. Hirai, S. Kumano, and T.-H. Nagai, *Phys. Rev. D* **71**, 113007 (2005); I. C. Cloet, W. Bentz, and A.W. Thomas, *Phys. Rev. Lett.* **102**, 252301 (2009).
7. O. Benhar, N. Farina, H. Nakamura, M. Sakuda, and R. Seki, *Nucl. Phys. B* **155**, 254 (2006).
8. W. Melnitchouk, R. Ent, and C. Keppel, *Phys. Rept.* **406**, 127 (2005).
9. M. Hirai, S. Kumano, and M. Miyama, *Phys. Rev. D* **64**, 034003 (2001).
10. M. Hirai, S. Kumano, and T.-H. Nagai, *Phys. Rev. C* **70**, 044905 (2004).
11. D. de Florian and R. Sassot, *Phys. Rev. D* **69**, 074028 (2004).
12. M. Hirai, S. Kumano, and T.-H. Nagai, *Phys. Rev. C* **76**, 065207 (2007).
13. I. Schienbein *et al.*, *Phys. Rev. D* **77**, 054013 (2008).
14. K. J. Eskola, H. Paukkunen, and C. A. Salgado, *JHEP* **0904**, 065 (2009).
15. S. A. Kulagin and R. Petti, *Phys. Rev. D* **76**, 094023 (2007).
16. L. Frankfurt, V. Guzey, and M. Strikman, *Phys. Rev. D* **71**, 054001 (2005).
17. J. M. Conrad, M. H. Shaevitz, and T. Bolton, *Rev. Mod. Phys.* **70**, 1341 (1998).
18. G. Önençüt *et al.* (CHORUS Collaboration), *Phys. Lett. B* **632**, 65 (2006).
19. M. Tzanov *et al.* (NuTeV Collaboration), *Phys. Rev. D* **74**, 012008 (2006).
20. See <http://minerva.fnal.gov/> for the MINERvA experiment.
21. J. Seely *et al.*, arXiv:0904.4448 [nucl-ex].
22. S. J. Brodsky *et al.*, *Phys. Rev. Lett.* **64**, 1342 (1990); *Phys. Rev. D* **70**, 116003 (2004).
23. L. D. Isenhower *et al.* (1999), E906 experiment at Fermilab, <http://p25ext.lanl.gov/e866/e866.html>.
24. S. Kumano, *Nucl. Phys. A* **782**, 442 (2007); *AIP Conf. Proc.* **1056**, 444 (2008).
25. S. Kumano, *Phys. Rept.* **303**, 183 (1998); G. T. Garvey and J.-C. Peng, *Prog. Part. Nucl. Phys.* **47**, 203 (2001).